Applied Catalysis B: Environmental 227 (2018) 102–113

Contents lists available at ScienceDirect

Applied Catalysis B: Environmental

journal homepage: www.elsevier.com/locate/apcatb

Engineered synthesis of hierarchical porous organic polymers for visible light and natural sunlight induced rapid degradation of azo, thiazine and fluorescein based dyes in a unique mechanistic pathway

Ipsita Nath[a], Jeet Chakraborty[a,1], Philippe M. Heynderickx[c], Francis Verpoort[a,b,*]

[a] Laboratory of Organometallics, Catalysis and Ordered Materials, State Key Laboratory of Advanced Technology for Materials Synthesis and Processing, Center for Chemical and Material Engineering, Wuhan University of Technology, Wuhan 430070, China
[b] National Research Tomsk Polytechnic University,Lenin Avenue 30, Tomsk 634050, Russia
[c] Ghent University Global Campus, 119 Songdomunhwa-Ro, Yeonsu-Gu, Songdo, Incheon 406-840, South Korea

ARTICLE INFO

Keywords:
Porous organic polymer
Dye degradation
Substrate selectivity
Photocatalysis
Hierarchical

ABSTRACT

We report the synthesis of two hierarchical organic polymeric networks for extremely efficient visible light and natural sunlight induced degradation of versatile wastewater organic contaminants under different simulated physical conditions following two distinct mechanistic protocols concomitantly. Tailored synthesis of the polymers by effective utilization of high-dilution-technique leads to extremely low density and hence high dispersibility of the networks featuring impressive surface area and gas adsorption abilities. UV–vis absorption spectra of both composites showed a significant coverage of the natural solar irradiance spectrum. A synthetic control over energy-state potentials allowed the materials to demonstrate an unprecedented dye pollutant degradation capability following two mechanisms, the conventional catalyst sensitized pathway, and a substrate-sensitized secondary pathway, simultaneously. Furthermore, the catalyst exhibited a unique time-dependent, sequential, in-situ alteration in substrate selectivity when subjected to a mixed-component pollutant probe. The photocatalytic ability retained essentially unaltered at outdoor condition under natural sunlight illumination as well as after five successive iterations. This work provides an experimental proof of the concept that strategic synthesis can be employed to control the physical and chemical properties of polymeric networks including their energy-states to achieve novel photo-responsive behaviour, and utilize them as green, sustainable environmentally benign and industrially viable heterogeneous catalysts.

1. Introduction

In recent years, semiconducting materials mediated photocatalysis have gained a surging interest for the removal of hazardous toxic substances from the environment through wastewater treatment, indoor air purification etc. in a green sustainable way [1,2]. Despite appreciable progress in the field, most of the materials lack the basic inherent necessities *viz.* an appropriate band-gap with proper valance band (VB) and conduction band (CB) potential configurations, effective exciton separation, and chemical stability [3,4]. Apart from these, a variety of metal oxides and/or other metal complexes that have been widely adopted as semiconductors till date, often suffer from substantial metal leaching, scarcity of natural resources as well as high price, and thereby limiting their utilization in practical purpose [5]. To this end, rationally tailored π–conjugated organic networks (known as porous organic polymers, POPs) fit well in all the aforementioned criteria and provide suitable semiconducting platforms [6]. POPs are permanently nanoporous three-dimensional materials with relatively high surface area and excellent thermal and chemical stability [7–17]. These structural features make them suitable candidates for highly recyclable heterogeneous catalyst working under even harsh conditions. It has been documented that highly disordered or even amorphous graphitic carbon nitride displays enhanced photoactivity due to effective suppression of the radiative electron-hole recombination [18,19]. Inherent amorphous nature of fully conjugated POPs thus manifests applications in light emission, light harvesting, optical sensing, and photocatalysis in a similar manner [20–26].

A variety of synthetic dyes have been widely used in the textile and printing industries with almost a million ton of annual production [27,90]. Azo dyes (e.g. methyl orange, MO; congo red, CR), thiazin (e.g.

* Corresponding author at: Laboratory of Organometallics, Catalysis and Ordered Materials, State Key Laboratory of Advanced Technology for Materials Synthesis and Processing, Center for Chemical and Material Engineering, Wuhan University of Technology, Wuhan 430070, China.
E-mail address: francis.verpoort@ghent.ac.kr (F. Verpoort).
[1] These authors have contributed equally to this work.

https://doi.org/10.1016/j.apcatb.2018.01.032
Received 13 October 2017; Received in revised form 31 December 2017; Accepted 15 January 2018
Available online 17 January 2018
0926-3373/

methylene blue, MB) and fluorescein based dyes (e.g. Rhodamine B, RhB) are the largest class used in the industry and their release in the environment imparts serious ecological damage because of the toxicity, non-biodegradability, potential carcinogenic and mutagenic nature of them [28–31]. Custom designed synthesis of most of these dye molecules possessing chromophore units with high bond energy (e.g. 407 kJ mol^{-1} for C═N in RhB, 518 kJ mol^{-1} for N═N in MO) [32] make them exceptionally stable, while their ionic structures contribute to high water solubility [33]. Moreover, the presence of these molecules in water significantly decrease the dissolved oxygen level increasing the BOD and COD, which further leads to potential damage of the aquatic life [34,35]. The traditional biological and physical treatment methods such as adsorption, ultrafiltration, coagulation etc. as well as advanced degradation processes of these molecules have met their limitations in some aspects including complex set-up, use of additional additives or peroxides etc. [36–41,90,91]. Therefore, to satisfy the practical need, semiconductor-induced photocatalytic decontamination of wastewater without the use of any additives is emerging as the green alternative.

Sun is the most abundant, clean and safe source of sustainable energy. Approximately 3×10^{24} J energy is delivered from the sun to earth per year, which is almost four times higher than the total annual energy consumption of humans all over the world [42]. Since visible light constitutes more than 45% of total sunlight, whereas hazardous UV light accounts for only 7%, researchers tend to focus on the utilization of visible light energy to carry out versatile transformations [43,44]. Nonetheless, these simulated visible light-induced reactions have enormous environmental advantages, the use of direct sunlight to promote such transformations, which is the ultimate goal for a green sustainable future, is still a long-standing dream [45–48]. In fact, examples of utilizing sunlight for chemical transformations are, to date, extremely rare in literature [49]. Development of a cost-effective and environment-friendly material that can efficiently harvest natural sunlight to promote chemical reactions on an industrial scale, as well as maintain a substantial recyclability is extremely desirable.

Till date, two mutually exclusive mechanistic approaches for the photo-generation of reactive catalytic species have been highlighted to degrade organic dye pollutants: the conventional and straightforward pathway requires the utilization of a semiconductor possessing narrow VB-CB energy gap that can be excited by visible light illumination [50–52], while the other method indulge the use of wide band gap semiconductors furnishing no feasible visible-light-induced activity by its own [42]. In this second method, dye pollutant, adsorbed on the catalytic surface, itself got excited after light illumination and injects that excited electron from their CB to that of the semiconductor to initiate the degradation [53]. Most of the metal based semiconductors and recently benzothiadiazole and polyoxometallate infused POPs have been widely exercised as the first type of materials [54–57], whereas a few surface modified TiO_2 and bismuth based materials are reported to exhibit the second type photoactivity [58–61]. To this end, we envisioned that engineered synthesis of appropriate POP skeletons possessing VB-CB energy gaps in the borderline region compared to the two abovementioned extreme cases should, in principle, bridge these two approaches and impart a unique concomitant photo-activation ability. To examine our proposed concept, we herein report the synthesis of two polymers, one containing no special photoactive unit and another one with azobenzene featuring good surface area and gas adsorption properties and studied the differences in their catalytic ability. Notably, in spite of several literature reports on photoresponsive character of azobenzenes, they have hardly been exercised as potential building units for polymeric semiconducting networks. It has also been documented that degradation of different classes of organic pollutants (cationic and anionic; azo, thiazine, fluorescein etc.) by any single photocatalyst is extremely difficult as they behave differently due to different surface properties [62,63,92,93]. The polymers reported here degraded aqueous solutions of RhB, MB, CR and MO almost quantitatively in a neutral, acidic and alkaline medium using visible light as an energy source with impressive reaction rate. More importantly, the identical catalytic ability was maintained in outdoor conditions under natural sunlight illumination indicating the sustainable industrial viability of the materials. Most surprisingly, an unprecedented time dependent in-situ alteration in substrate selectivity was observed during degradation of a mixed-dye pollutant probe, which established the feasibility of our proposed concept. To the best of our knowledge, this is the first ever POP-based semiconductor mediated photocatalytic study to address the degradation of a wide variety of environmentally hazardous organic pollutants following a tactically unique mechanistic protocol under visible as well as natural sunlight illumination.

2. Experimental section

2.1. General methods

Solid state ^{13}C-CP/MAS NMR spectra analysis were measured on a Bruker Advance 400 DSX spectrometer operating at 100 MHz for ^{13}C and 400 MHz for ^{1}H. ^{1}H-^{13}C Cross Polarization Magic Angle Spinning (CP/MAS) were performed at MAS of 10 kHz in a 4 mm zirconia rotor. TPPM decoupling was used for acquisition. The values of chemical shifts are given referenced to TMS. FT-IR spectroscopy was carried out on a Bruker Vertex 80 V FT-IR spectrometer. Powder XRD analyses were performed on a Bruker D8 Advance diffractometer with a copper Kα radiation source (λ = 1.54056 Å) at 40 kV and 45 Ma with 5°/sec scanning speed. The adsorption desorption isotherms were analysed by Micrometrics instrument (ASAP 2020) using ultrapure N_2, CO_2 and CH_4 (99.999%) at 77.3 K. Samples were degassed at 150 °C for 2 h at vacuum prior analysis. Surface area values were calculated using Brunauer-Emmett-Teller (BET) and Langmuir methods at $0.003 < P/P_0 < 0.05$ range. Pore size distributions were calculated from N_2 sorption isotherms using the nonlocal density functional theory (NLDFT). Thermal gravimetric analyses (TGA) were carried out on a Netzsch STA 409 thermal analyser under an inert atmosphere at a heating rate of 10 °C/min from room temperature to 1000 °C. The morphology studies were conducted by Scanning Electron Microscopy (SEM) on a JEOL JSM-5610LV (0.5–35 kV) microscope. TEM analysis was carried out using a Philips CM20 microscope at 200 kV. Imaging and diffraction of the structure was performed at low electron dose for minimising beam damage to the sample. The binding energies of the elements present in the polymers were measured by X-ray photoelectron spectroscopy (XPS) on Thermo Fisher ESCALAB 250Xi. UV–vis absorptions of polymers were recorded in solution state on a Shimadzu UV-1800 UV–vis spectrophotometer using a 10 mm path length quartz cuvette at room temperature. 1 mg POPs were dispersed in 3 mL water by ultrasonication prior measurement. Electron paramagnetic resonance (EPR) was measured on Bruker PMX spectrometer at room temperature. Cyclic voltammograms were taken on CHI-660E electrochemical workstation. Total organic carbon (TOC) analyses were performed by a VarioTOC instrument (liquid mode).

2.2. Synthesis

Monomer 1,2-bis(3,5-dibromophenyl)diazene was prepared following reported literature procedure [64]. POP-1 and POP-2 were prepared by Sonogashira-Hagihara cross-coupling of 1,4-diethynylbenzene (1.5 eqv.) and corresponding aryl bromides (1 eqv.) in the presence of tetrakis(triphenylphosphine) palladium (0.05 eqv.) and cuprous iodide (0.08 eqv.) in 3:1 mixture of DMF and triethylamine at 80 °C for 72 h under inert atmosphere (Scheme 1). 1,3,5-bromobenzene reacted with 1,4-diethynylbenzene to afford POP-1 network, whereas 1,2-bis(3,5-dibromophenyl)diazene gave POP-2. The solid products obtained after the reaction was repeatedly washed with water and acetone, then treated with methanol and acetone in a Soxhlet for 24 h and dried under vacuum. Both POP-1 (yield 98%) and POP-2 (yield 95%) appeared as yellowish brown powder insoluble in common

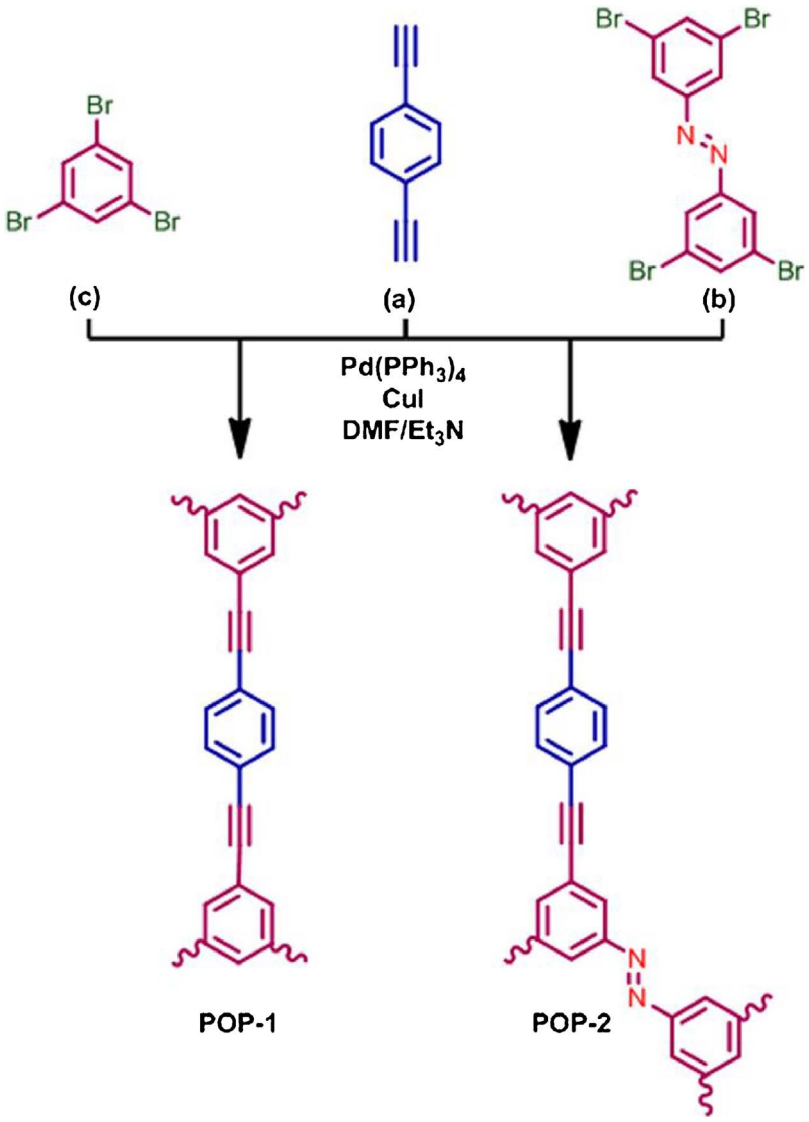

Scheme 1. Synthetic route to POP-1 and POP-2 starting from respective monomer (b, c) and co-monomer (a).

solvents. ICP-MS analysis of the materials showed 20 and 25 ppm Pd was present in POP-1 and 2 respectively, whereas Cu contents were 12 and 15 ppm only.

2.3. Photocatalytic activity measurements

Photocatalytic activities of POP-1 and POP-2 were evaluated by photodegradation of RhB, MB, CR, MO, and a mixture of MB and MO. Due to the difference in absorptivities, aqueous solutions of RhB and MB were prepared at 10 ppm concentration whereas 25 ppm concentrations were maintained for CR and MO. Finely powdered catalysts (1 mg/mL) were dispersed in dye solutions and the suspension was stirred in the dark for 2 h prior subjecting to light, to achieve the adsorption desorption equilibrium. It was then exposed to a PL-XQ 350W Xe lamp attached with a long-pass UV cut-off filter ($\lambda > 420$ nm). The distance between the lamp and the dye solutions was maintained to be 10 cm. To nullify the temperature effect, the whole experiments were carried out in a water bath at room temperature. After a required time the suspensions were centrifuged to separate solid catalysts from the solution. It was then transferred to a quartz cuvette and UV–vis absorption spectra were measured on a Shimadzu UV-1800 spectrophotometer. The degradation efficiencies were evaluated by monitoring the gradual decrease of the intensity of maximum absorption peaks. The controlled experiments were performed following similar procedures with added scavengers (1 mmol/L). For reusability, the catalysts were separated by centrifugation, washed four times with water and used directly in a subsequent run.

3. Results and discussion

Sonogashira-Hagihara cross-coupling of 1,4-diethynylbenzene (DEB) with monomers 1,3,5-tribromobenzene and 1,2-bis(3,5-dibromophenyl)diazene resulted in two polymeric networks, POP-1 and POP-2 respectively. Both polymers appeared as yellowish brown amorphous powder insoluble in common solvents. Initial synthetic approach with a minimum volume of DMF as solvent afforded a required network of POP-1 possessing BET surface area as high as 740 m^2g^{-1} (Langmuir area 817 m^2g^{-1}) with a pore volume of 0.5 cm^3g^{-1} (data not shown). The t-Plot micropore area measurement further revealed that more than 60% of the skeleton consisted of micropores. This was in accordance with NLDFT pore size distribution with maximum pore density in the ultra-microporous region (< 1 nm). Due to the requirement of an appreciable amount of large pores in a well-performing heterogeneous catalyst for efficient mass diffusion of reactants and products, we employed the application of high dilution technique for synthesizing polymer networks. It was envisioned that such technique would decrease the local concentration of monomers and co-monomers and allow them to uniformly distribute over a large

bulk leading to a relatively less inter-penetrated network. Contextually, this method is widely employed for homogeneous long-chain cyclization reactions and in Zeolitic Imidazole Framework synthesis for similar reason [65–67]. Accordingly, small loose flake type products started to appear throughout the whole reaction mixture after a certain time which was in stark contrast to the previous observation where most of the mixture solidified after a few minutes. The products, prepared by this high dilution protocol, essentially possessed very low density, hence highly dispersed in common solvents and very difficult to wash by centrifugation. Synthesis of POPs are kinetically controlled and goes through step by step formation of macrocyclic intermediates which then joins together to yield the whole network [68]. High dilution technique offers these intermediates a chance to minimize their torsional strains leading to the attainment of sufficiently low energetic conformations. Therefore, it forbids immediate coupling of any intermediate to its adjacent ones and decreases overall reaction rate. This theory explains the necessity of a longer reaction time and low density of the products.

The FT-IR analysis of both polymers demonstrated peaks near 2200 cm^{-1} ascertained to the characteristic C≡C stretching, confirming successful coupling of the monomers with DEB (Fig. S1). The absence of any free terminal acetylene unit was further confirmed from the disappearance of the strong sharp peak near 3250 cm^{-1}, characteristic to the alkyne C—H stretching. Aromatic C—H stretching of both POP-1 and POP-2 also gave peaks near 3000 cm^{-1}. Generation of these organic networks was assessed additionally from solid-state ^{13}C cross-polarization NMR analysis (Figs. S2 and S3). Acetylene carbons of POP-1 appeared at 90 and 92 ppm, while that for POP-2 came at 89 ppm respectively. Resonances for proton bearing aromatic carbons were found at 123 ppm, whereas peak at 131 ppm was ascribed to the aromatic carbons directly attached to the adjacent acetylene units. POP-2 features another peak at 152 ppm resulted from the carbon bonded to N-atom of the azo group. Elemental analysis of POP-1 showed 96.27% of its structure consists of C whereas H is 3.398%. Similarly, POP-2 was found to contain 90.32% C, 3.485% H and 6.695% N. These values match well with the theoretically assessed structure (Table S1), confirming their successful generation. The thermogravimetric analysis (TGA) of the polymers revealed that they are exceptionally stable (Fig. S4). POP-1 showed a slight decrease of ~4 wt% at 100 °C possibly due to the removal of some trapped solvents and then maintained its structural integrity till 300 °C. A subsequent steady decrease of ~17 wt % was observed till 1000 °C with almost 80% remaining residual mass. POP-2 also maintained an intact structure till 300 °C, and then suffered ~40 wt% weight loss from 300 to 1000 °C with 60% residual remaining. This confirmed the excellent thermal stability of both POPs till 300 °C and even at much higher temperature the structures did not collapse completely. The broad patterns in the powder X-ray diffraction study indicated amorphous nature of the materials (Fig. S5).

Morphologies of the polymers analysed by FESEM are demonstrated in Fig. 1. POP-1 appeared as small sheets of ca. 100–200 nm size. It can be observed that small layered flakes joined together to give the morphology. Irregular spherical or bean type architectures were detected for POP-2. The presence of lamellar sheets can be seen in Fig. 1. The earlier discussed observation of the appearance of small loose flakes in the reaction mixture during synthesis can be reasoned for the layered structures of both polymers. TEM images of both materials (Fig. S6 and S7) also confirmed their said morphology and amorphous nature.

The surface areas and porosities of the materials were determined by N_2 adsorption-desorption isotherm at 77 K. According to the latest IUPAC convention, both polymers demonstrated Type II isotherms (Fig. 2a) as indicated by their typical shape resulted due to unrestricted monolayer-multilayer adsorption till high P/P_0 value [69]. The BET surface areas of POP-1 and POP-2 were found to be 639 and 281 $m^2 g^{-1}$ (Table S2) with pore volumes of 0.46 $cm^3 g^{-1}$ and 0.50 $cm^3 g^{-1}$ respectively. Steep N_2 uptake by the polymers at low relative pressure region is indicative of the presence of an appreciable number of

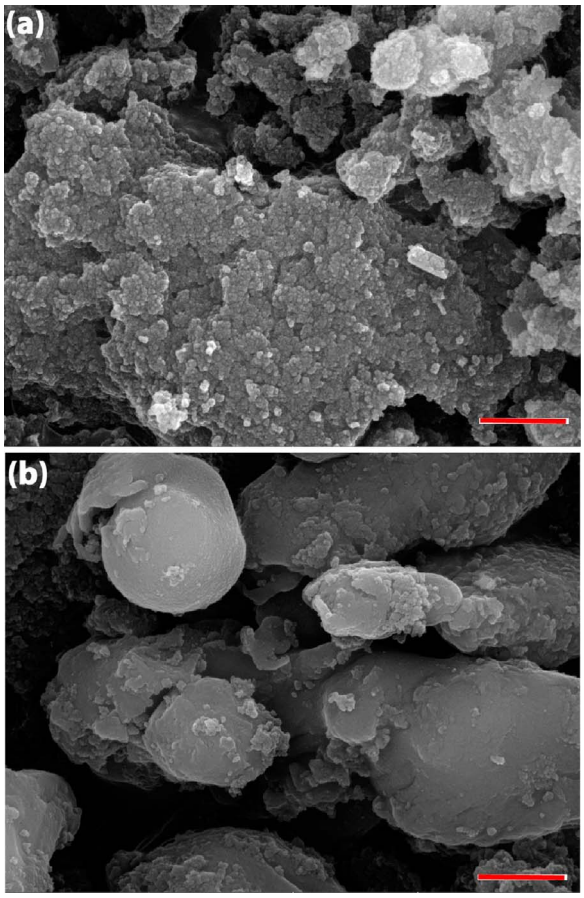

Fig. 1. FESEM image of (a) POP-1; (c) POP-2. The bar scale in both images is 2 μm.

micropores. A less distinctive inflection with a gradual curvature at the beginning of the middle section infers substantial overlap of monolayer and multilayer adsorption. The moderate slope of the otherwise linear middle section further confirms this concomitant monolayer and multilayer adsorption. A certain increase in adsorption was observed when P/P_0 reached their limiting maxima due to an increase of the thickness of adsorbed multilayers, which is the characteristic feature of Type II isotherm, for both polymers. On the other hand, a large hysteresis at the higher relative pressure region can be accounted for additional mesoporosity in POP-1 and POP-2. NLDFT pore size distribution also confirmed the presence of micro and mesopores in the structures. It can be seen that both materials featured a maximum pore density at 1.74 and 2.07 nm, while POP-1 has an additional maximum at 1.07 nm. This explains its steep N_2 adsorption at low pressure and higher BET compared to POP-2. Interestingly, a wide set of mesopores possessing diameters in the range of 2.45–5.01 nm were observed in the materials signifying their structural hierarchy and augmented catalytic propensity. The t-plot analysis further revealed that almost 55% of the total surface area of POP-1 came from micropores, whereas POP-2 consists of ~39% micropores. The BET plots (Fig. 2b, Table S3) showed an exceptional goodness of fit with 0.999 R^2. Compared to the initially synthesized material discussed at the beginning of this section, polymers prepared by high dilution technique possessed a strikingly different porosity distribution. According to our anticipation, the technique allowed the generation of a large number of mesopores with the expense of a significant decrease of ultra-micropores and ipso facto the suppression of surface area.

3.1. Carbon dioxide and methane uptake

CO_2 and CH_4 sorption isotherms of the polymers were measured at

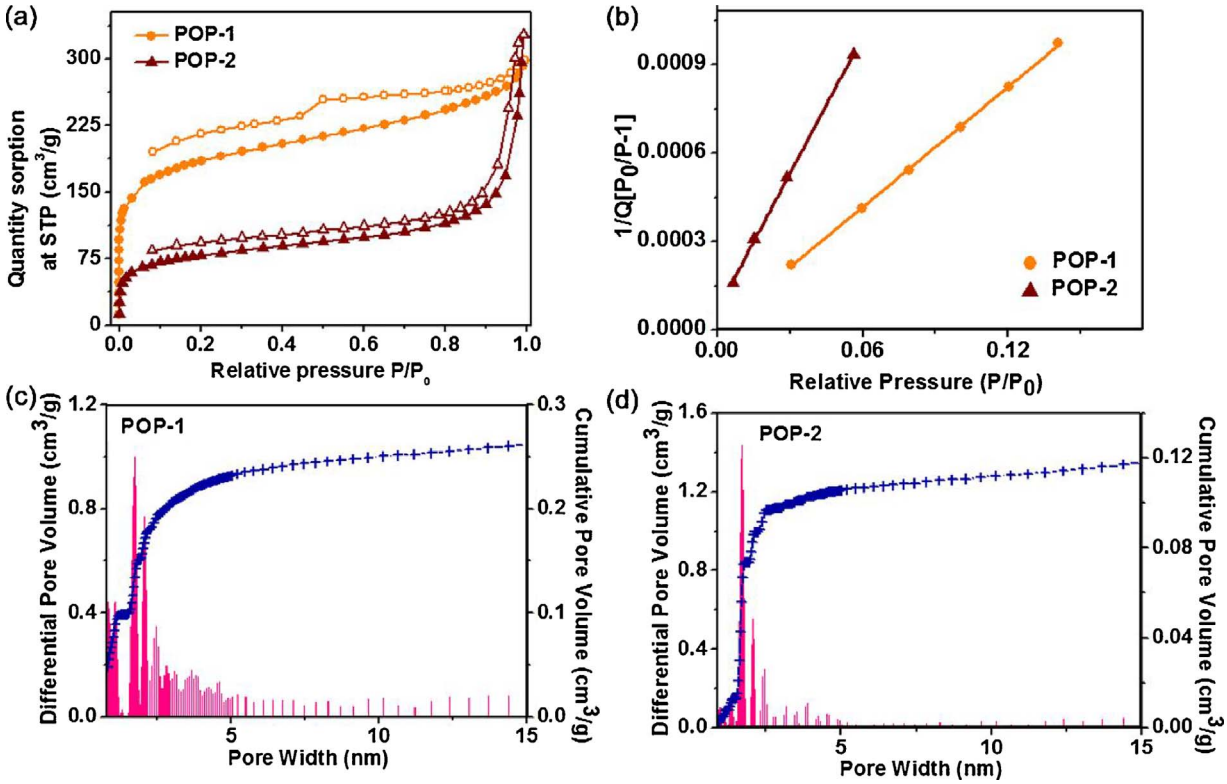

Fig. 2. Surface area and porosity plot of the polymers. (a) Sorption isotherms; (b) linear fit of BET surface area of POP-1 and POP-2; (c) porosity distribution of POP-1 and (d) porosity distribution of POP-2.

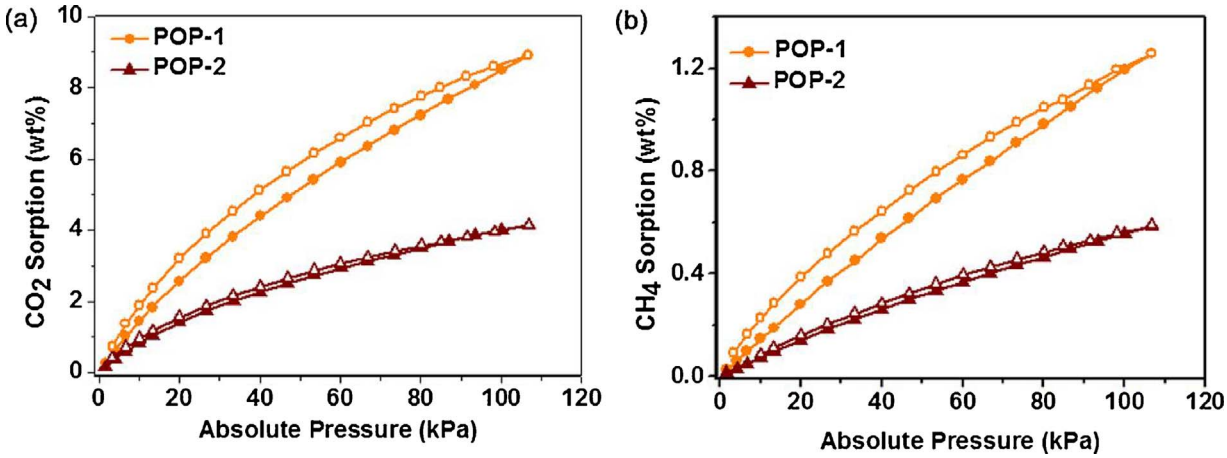

Fig. 3. (a) CO_2 and (b) CH_4 sorption isotherms of POP-1 and POP-2.

273 K and 1 bar pressure (Fig. 3). POP-1 exhibited highest CO_2 uptake of 9 wt% which is comparable to most of the reported POPs for selective CO_2 adsorption [70–73]. Despite possessing nitrogen containing structural units, POP-2 showed only 4 wt% CO_2 uptake. Though interactions between CO_2 and porous nitrogen containing networks are reported to favour CO_2 adsorption capacity, low surface area and lack of sufficient small micropores in the structure could be reasoned for the nominal uptake-ability of POP-2. On the other hand, due to the presence of ultramicropores (~1 nm) in POP-1, as discussed earlier, CO_2 adsorption through multiwall interaction could lead to higher uptake [74]. The presence of a large hysteresis in the CO_2 sorption isotherm in POP-1 compared to the other polymer also suggests the possibility of multiwall interaction. Finally, the higher BET surface area could have contributed to the larger CO_2 uptake of POP-1 to some extent [75]. The CH_4 uptake capability of the materials also followed a similar trend with POP-1 and POP-2 exhibiting 1.2 and 0.5 wt% adsorption respectively.

3.2. Photophysical and electrochemical properties

Steady-state absorption spectra of the polymers were measured in the aqueous solution state. Irrespective of different structural units, both POP-1 and -2 showed absorption maxima near 380 nm. Nonetheless, POP-1 showed a broad absorption peak compared to POP-2. It can be noted from the UV–vis absorption pattern of the materials shown in Fig. 4a, that both of them possess a significant absorbance even at 900 nm wave length. Efficient coupling of the monomers and co-monomers using high dilution technique is anticipated to increase overall conjugation of the network leading to this highly absorbing tail even at near-IR range. The VB potentials of the polymers obtained from XPS analysis demonstrated that POP-1 featured a VB at 1.56 V while a

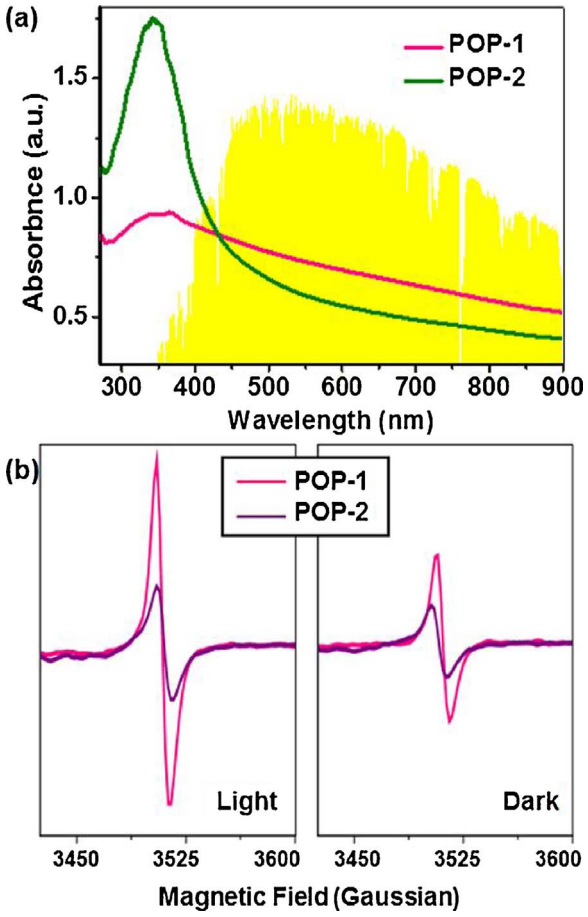

Fig. 4. (a) UV–vis absorption pattern (solution state) of the aqueous dispersion of POPs with natural solar irradiance spectrum till 900 nm (background); and (b) EPR spectra of the polymers in the presence (right) and absence (left) of light.

1.85 V state energy was found for POP-2 (Fig. S10). The cyclic voltammogram experiment, on the other hand, revealed that the CB potential of POP-1 was −1.31 V (vs. GCE), whereas POP-2 possessed a CB at −0.92 V (vs. GCE) respectively (Figs. S8 and S9). From these values, corresponding electronic band gaps of the polymers were calculated to be 2.87 and 2.77 eV.

Electron paramagnetic resonance (EPR) was also employed to investigate the unpaired electrons in the polymeric systems in the presence and absence of visible light illumination, respectively. As depicted in Fig. 4b, a single Lorentzian line was detected for each of the samples indicating the generation of an electronic conduction in the conjugated π-system localized over the whole structure of both polymers [76]. The increase of the intensity of these spectral lines after visible light illumination inferred an overall increase of the conjugation of electron stimulated by light energy. It can be observed that POP-1 produced a more prominent and intensified line compared to POP-2 under either condition which is consistent to its lower energy gap.

3.3. Assessment of photocatalytic activity

Organic dye molecules are emerging as a class of potentially hazardous water pollutants. The synthesis of a material having the ability to annihilate these compounds irrespective of their different chemical and surface properties, using cheap, abundant and completely green solar light is highly desirable. To achieve this goal, POP-1 and -2 were subjected to degrade the aqueous solutions of RhB, MB, CR, and MO under visible as well as natural sunlight without using any additives or peroxides (Figs. S16 and S22). Owing to the highly hierarchical porous nature of both polymers, a significant adsorption of dyes onto their surface was expected. Therefore, to exclude the role of simple adsorption from the overall degradation pathway, the suspensions of the photocatalysts in dye solution were kept in the dark for 2 h with continuous stirring to ensure the achievement of an adsorption-desorption equilibrium. It has been reported that it is difficult for any single catalyst to degrade both anionic and cationic dye pollutants with equal ease as they show completely different surface properties under identical conditions [62,63]. Degradation of azo dyes, especially if it goes via the breaking of high-energy N=N bonds, is particularly difficult [77,90]. To evaluate the propensity of our materials for degrading all these pollutants, the half-life ($t_{1/2}$, time required to decrease the initial dye concentration C_0 by half) and degradation efficiency ($\eta = (1 - C/C_0) \times 100\%$, where C is concentration at time *t*) were measured for an easy numerical comparison (Table 1).

Table 1
Degradation efficiency, rate constant and half-life of different dyes catalysed by POP-1 and POP-2 under visible light illumination.

Catalyst	Dye	Degradation efficiency (%)	Initial rate constant (k_{obs} in $\times 10^{-3}$ min^{-1})	$t_{1/2}$ (min)
POP-1	RhB	> 99	67	11
	MB	> 99	43.5	18
	CR	90	22.3	28
	MO	91	6.5	71
POP-2	RhB	90	39.1	16
	MB	96	24.7	28
	CR	67	31.5	22
	MO	2	N.A.	N.A.

3.4. Visible-light-induced dye degradation

To understand the photo-induced degradation pathway of the organic water-pollutants in the presence of semiconducting catalysts, we fitted the rate curves in a simplified pseudo-first-order kinetic model given by Eqn. 1 which is consistent with literature reports [78–81].

$$C/C_0 = \exp(-k_{obs}t) \quad (1)$$

where k_{obs} is the observed reaction rate constant and *t* is the time of reaction measured in minutes. The degradation curves for all four dye pollutants catalysed by POP-1 and POP-2 are depicted in Fig. 5. It can be noted that the degradations followed pseudo-first-order rate at the initial stage, but deviates later at a low C/C_0 region. This apparent deviation from the expected model can be explained considering that after a certain time, the concentration of dyes decreased substantially compared to the dissolved O_2. Under such circumstances, the consideration of the pseudo-first-order rate model does not hold true anymore [78].

It is evident from the rate plots that POP-1 exhibited better catalytic performance than POP-2 for degrading the dyes (Fig. 5). Owing to the deviation from the proposed first order model, calculation of overall reaction rate constant remained challenging. The initial reaction rates are calculated instead from the linear fitting of $\ln(C/C_0)$ vs. time as depicted in Table 1. It can be seen that for both catalysts, the initial rates of RhB degradation are higher than that of MB. However, MB demanded far less time for its complete removal compared to RhB. A similar phenomena could also be observed for the degradation of CR, where despite having higher initial reaction rate, POP-2 failed to demonstrate a better activity than POP-1. In fact, after achieving a fast 60% degradation efficiency, its reaction rate decreased abruptly. Almost quantitative efficiency was attained by POP-1 for degrading RhB and MB within as low as 75 min and 45 min respectively. Whereas, under identical conditions, POP-2 yielded more than 90% conversions at relatively higher reaction times. Moreover, a steady 90% reduction in MO concentration was also accomplished under investigated conditions by POP-1, while employment of POP-2 resulted in insignificant

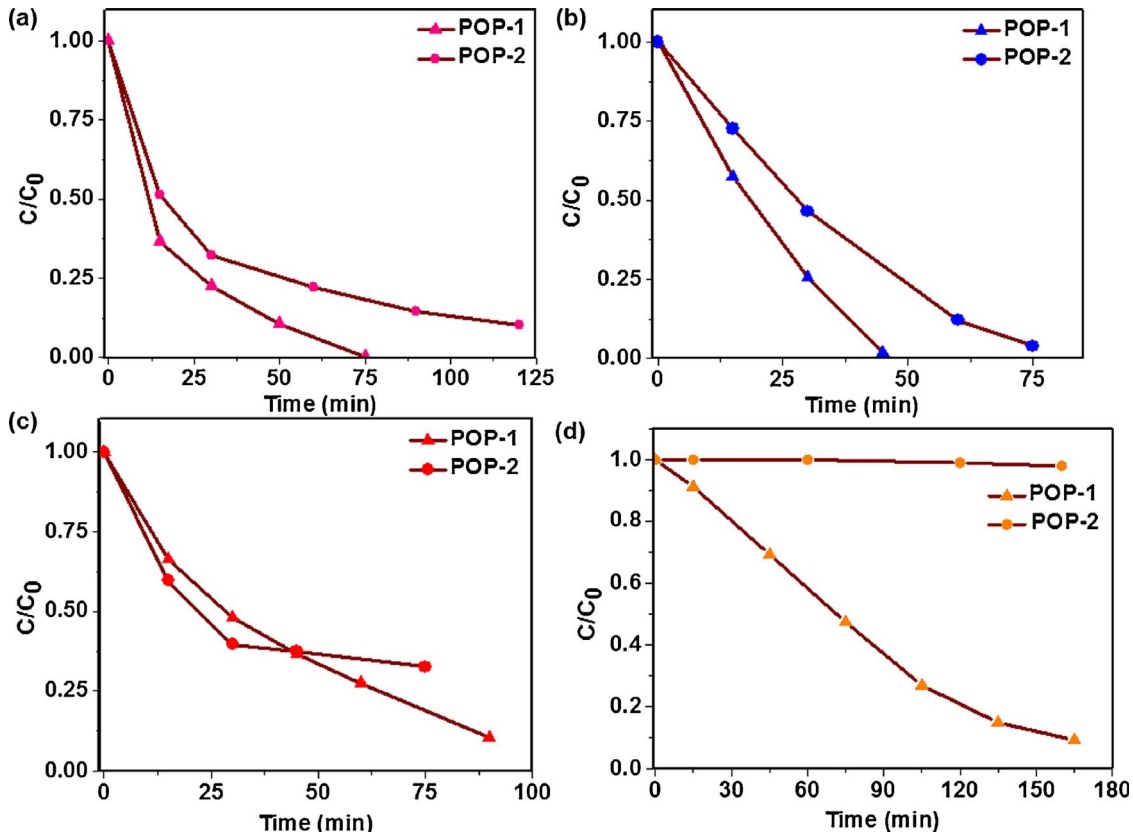

Fig. 5. Rate plots for the degradation of (a) RhB; (b) MB; (c) CR and (d) MO catalysed by the POPs.

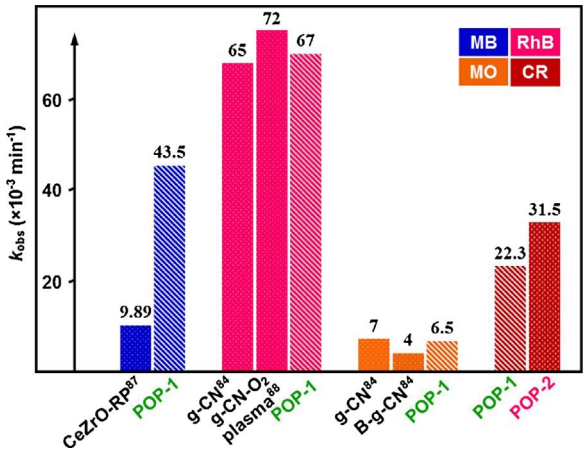

Fig. 6. A comparative study of the degradation rates of various dyes by reported catalysts and our catalytic systems at neutral pH.

degradation. $t_{1/2}$ can be considered as an easy tool for a qualitative assessment of the catalytic ability. POP-1 showed considerably low $t_{1/2}$ for the cationic dyes. On the other hand, anionic azo dyes took comparatively more time for their skeletal destruction. It should also be noted that during this catalytic study the dye/catalyst ratios for the azo dyes were 2.5 times higher than that for the cationic dyes. This can also be considered as one of the reasons for their slow reaction rate. In order to propose the amenability of our catalytic system with respect to other conventional and novel photocatalysts, a comparative diagram of reaction rates for the removal of different dyes are illustrated in Fig. 6 and Table S4. Our systems were found to follow exceptional catalytic ability under visible light illumination for all kinds of dyes. Moreover, mineralization efficiency of the catalysts were analysed in terms of the reduction of the total organic carbon (TOC) contents of each dye solutions measured before and after degradation process. The%reductions of TOC values are depicted in table S5 confirming the excellent efficiency of both catalysts.

The change in absorption spectra of the dyes on photo-treatment in the presence of polymer catalysts and their corresponding shifts in λ_{max} are illustrated in Fig. 7 (and Figs. S12–S15). Absorption peaks at higher λ region correspond to the n–π* transition of the dyes originated from the chromophore units, whereas the peaks at lower λ values are generated due to the π–π* transition of the overall aromatic structures. Though the absorption intensities were almost quantitatively quenched for every investigated pollutant probes, only RhB and MO exhibited an appreciable hypsochromic shifts of λ_{max}. However, the positions of the absorption bands were also blue shifted for MB and CR to a nominal extent. Based on this behaviour of the absorption plots, a qualitative assessment of the plausible mechanistic protocols can be drawn. Comparing relevant literature with similar documented observations [42,58,63,81–83,94], it can be inferred that RhB and MO may have been degraded by an N-dealkylation pathway. Evidently, N-dealkylation leads to a significant change in the chemical structures of the dye pollutants (Fig. S11), which in turn affect the overall conjugation of the electronic clouds. A gradual shift in λ_{max} often arises due to this phenomena. N-demethylation of the RhB skeleton and similar N-demethylation of MO accordingly resulted in a blue shift of respective λ_{max}. Interestingly, instead of a gradual movement of the absorption bands observed for RhB and CR, MO manifested a certain sharp change at a later stage of the reaction (Fig. 7). This may be explained by considering a steady destruction of the dye skeletons of RhB and CR over time, while MO experienced an acute structural collapse after a required reaction time owing to the implicit difficulty of destroying the N=N azo bond. Complete removal of the bands originated from n–π* and π–π* transitions under our investigated conditions evidently indicates that the photocatalysts are capable to destroy the chromophore units as well as the overall structures of the dye molecules. Due to the

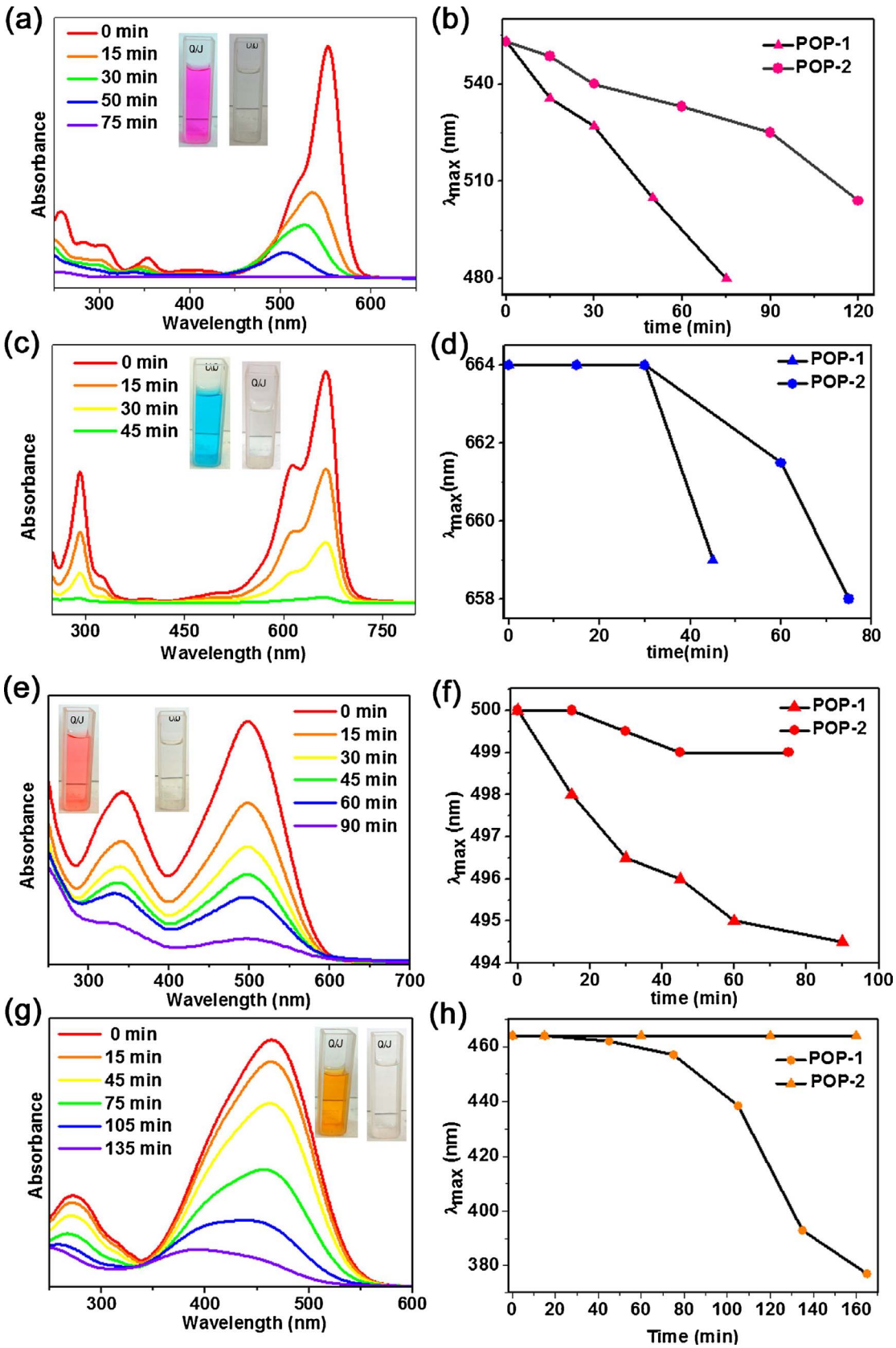

Fig. 7. UV–vis absorption patterns of (a) RhB; (c) MB; (e) CR and (g) MO degradation catalysed by POP-1 at different visible light illumination times and the digital images of respective dyes before and after degradation (inset). Shift in λ_{max} during degradation of (b) RhB; (d) MB; (f) CR; and (h) MO over different reaction times catalysed by both polymers.

low energies of C—C and C—N bonds, it was easy for the catalysts to destroy those bonds at the beginning of the degradation, while with progressive time, high energy C═N and N═N bonds had also been successfully destroyed [63]. Different adsorptivities of any particular catalyst for different dyes can also possibly lead to its distinctive catalytic performances.

4. Adaptability

4.1. Effect of pH

For sustainable industrial and field applications, materials with higher tolerance in different environments and good recyclability are always preferred [77]. The varying pH of the wastewater is often found as one of such circumstances that make the degradation of dissolved pollutants immensely difficult. For example, most of the anionic azo dyes are very difficult to degrade in alkaline media, and with an increase in pH, the degradation efficiency severely deteriorates [81,91]. Removal of MO from the alkaline medium is particularly difficult. However, under acidic condition, most of these azo compounds undergo a proton mediated structural alteration which makes them relatively easy candidates for degradation. The reverse effect is true for the cationic dyes as a higher pH facilitates their structural collapse while they remain almost intact in an acidic solvent. Owing to the exceptional ability of POP-1 to completely remove all kinds of dyes from their as prepared solutions, we further employed it to investigate its extended applicability under harsh acidic and alkaline conditions. Accordingly, MB and MO were probed as two prototypes and their degradation efficiencies and patterns were checked for the as prepared solutions of pH 7 (for MO) and 6 (for MB), as well as at pH 2 and 10. As evident from Fig. 8, change in pH imparted only a slight effect on the removal of MB

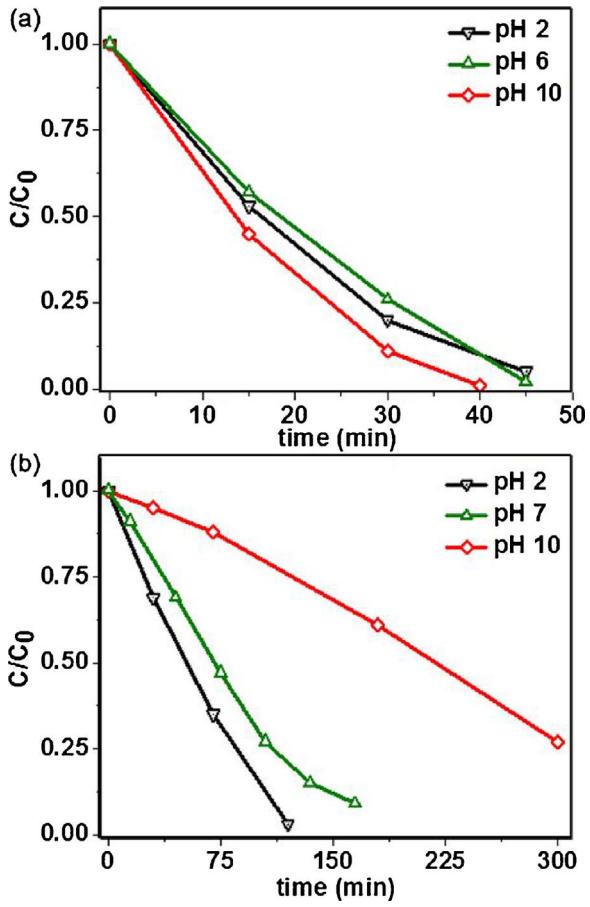

Fig. 8. Degradation rate profile of (a) MB and (b) MO catalysed by POP-1 at variable pH.

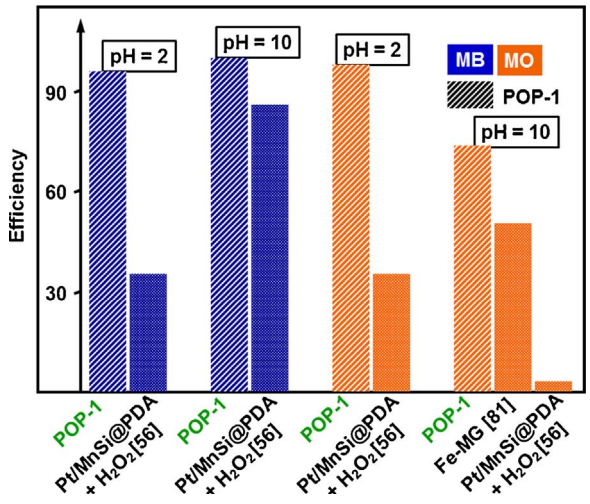

Fig. 9. A comparative study of degradation efficiency of MB and MO at acidic and alkaline media catalysed by previously reported semiconductor systems and POP-1.

as an almost quantitative reduction in concentration was observed within 40–45 min. Nonetheless, the alkaline solution degraded relatively quickly while a trivial decrease in reaction rate over time was observed at pH 2. On the other hand, degradation efficiency of MO highly relied upon the pH of the medium. Under the acidic condition, a fast reaction rate was observed possibly due to the aforementioned structural change, while with an increase in pH value the rate gradually decreases. At extremely alkaline medium of pH 10, 74% decrease in dye concentration was observed after 5 h. To the best of our knowledge, this is still the highest performance among similar reported catalytic conditions [56,81,84]. Moreover, it can be seen from the degradation curve that at alkaline medium the reaction followed a completely different rate law compared to neutral or acidic pH explaining the requirement of longer reaction span. A comparative diagram of the efficiency of different reported catalysts to our catalytic system performing under highly acidic or alkaline medium has been given in Fig. 9. Evidently, POP-1 demonstrated far superior activity under either conditions.

4.2. Selective degradation

Selective degradation of pollutants imparts a crucial role for their targeted removal from the environment. Selective reactivity of catalysts based on the surface charges of the reactants, therefore, attracts a lot of research interests [56,85]. The relatively less activity of POP-2 for the azo dyes compared to cationic RhB and MB intrigued us to cultivate the possibility of selective degradation of a cationic dye from a binary mixture. Owing to the highest and least activity of POP-2 for degrading MB and MO respectively, a mixture of these two dyes with MO possessing 2.5 times higher concentration than MB, was employed as a prototype. Surprisingly, contrary to our anticipation more than 85% MO was found to be degraded within first 15 min of the reaction with essentially no decrease in MB concentration (Fig. 10). This phenomenon showed an unexpected and unprecedented reverse selectivity in an anionic-cationic binary mixture by POP-2. While examples of conventional selective removal of dyes are abundant [56,85], such in situ alteration in substrate selectivity without changing any reaction conditions are extremely rare. On advancement of reaction time, a gradual decrease in MB concentration was observed and almost a clear solution was obtained after 1 h. This observation further indicates that POP-2 is able to manifest a time dependent selective reactivity in a mixture of different substrates.

A set of reaction conditions were screened further for better understanding of this phenomena. Alteration of the MB and MO concentrations in the binary mixture showed similar selective degradations

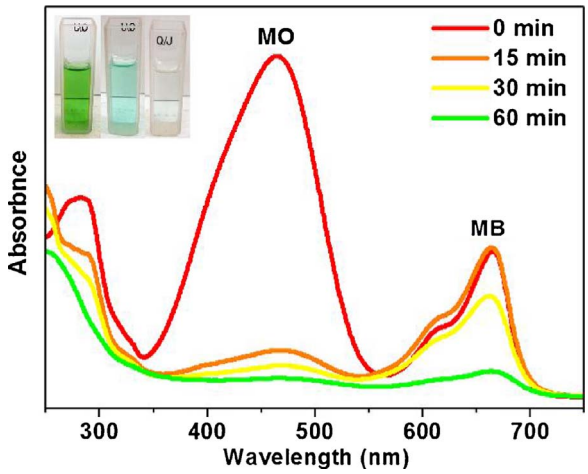

Fig. 10. UV–vis absorption pattern for a time dependent selective degradation of MO and MB in a MO + MB binary mixture by POP-2. (Inset) digital photograph of the mixture at the beginning; after 15 min; and at the end of reaction.

by POP-2. When the initial MB/MO ratio was maintained at 0.6 a fast removal of MO was observed (Fig. S19c), whereas a higher MO concentration required more time for removal (Fig. S19d). However, the initial selectivity towards degradation of MO was maintained irrespective of the individual dye concentrations. A subsequent complete removal of MB occurred in both experiments as well. POP-1 was then targeted as the catalyst to test if it too can manifest a similar selective degradation pattern in the binary mixture. To our delight, within first 10 min a rapid removal of MO was observed along with almost complete degradation of MB. As MB was removed, the resultant solution containing mostly MO was further degraded in a relatively slow reaction rate (Fig. S19a). This observation confirmed that POP-1 also possessed a selective removal ability for MO in the presence of MB. However, as soon as MB was removed from the solution, the remaining MO was degraded by POP-1 in a normal course. Moreover, instead of MB, when a RhB + MO mixture was employed with POP-2, a gradual decrease in the concentrations of both dyes was monitored indicating that the presence of RhB can impart MO degradation ability in POP-2 as well (Fig. S19b). These experiments all together indicates that both POPs were able to manifest a selective reactivity in a binary mixture.

4.3. Mechanistic explanation

For a clear understanding of the reactive species involved in our dye degradation experiments and their plausible generation, control experiments were carried out to test their effects on the removal efficiency of RhB using both polymers. Only a little conversion in an inert atmosphere after required time clarified the vital role of O_2. Since a variety of reactive oxygen species (ROS) are known to affect the photoactivity of semiconductor materials; benzoquinone, sodium azide and isopropanol were employed as typical $O_2\cdot^-$, $^1O_2$ and $OH\cdot$ scavengers respectively. As shown in Fig. 11, $O_2\cdot^-$ was found to possess most significant effect in the removal of dyes with little contributions from other ROS. Most interestingly, when potassium iodide (KI) was employed as the hole scavenger, a rapid degradation was observed with an exceedingly fast rate. Typically, in the presence of KI, the reaction took only 1/3rd of its original time to achieve completion. Such behaviour can only be explained considering that addition of KI highly restrained the recombination of excitons [63]. The direct recombination and surface recombination of electrons and holes in an excited semiconductor may result in reduced efficiency of the photocatalytic system. When the photogenerated holes were scavenged by KI, the excited electrons in the CB of the photocatalyst were left with no option but reacting with aerial O_2 to generate ROS in a higher degree, leading to

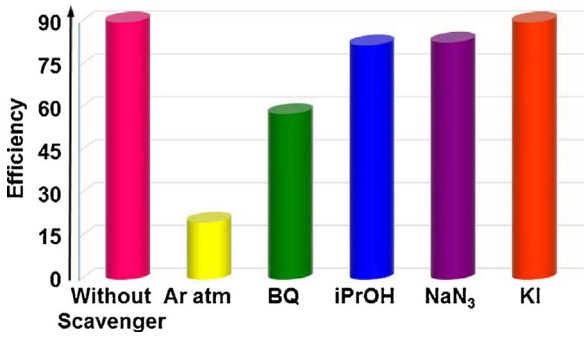

Fig. 11. Role of different scavengers on the degradation efficiency of RhB catalysed by POP-1 after 50 min of reaction.

the rapid degradation of dyes. This phenomenon de facto provides a supporting proof of the direct visible-light-induced excitation of the photocatalysts. The ability of the polymers to generate ROS under visible light irradiation at room temperature were further assessed by EPR spin-trapping experiments. Employment of 5,5-dimethyl-1-pyrroline-N-oxide (DMPO) confirmed that both materials were susceptible to generate $O_2\cdot$ (Fig. S17), whereas the use of 2,2,6,6-tetramethylpiperidine (TEMP) showed that POP-1 can produce $^1O_2$ as well (Fig. S18). This may explain the superior catalytic activity of POP-1 over POP-2.

Nonetheless, considering that POP-2 exhibited no catalytic ability for the removal of MO, but degraded the same dye in a rapid and selective manner from the binary mixtures of MO and MB, it is evident that a different mechanistic approach needs to be taken into account to analyse the occurrence. It was also observed that the polymers were able to adsorb MO in only trace amounts whereas adsorption abilities for other dyes were relatively higher. With these observations in hand, the adsorbed dye-assisted or dye-sensitized degradation pathway can be considered as the only reasonable justification for such unpredicted activity. Such phenomena have been reported, though rarely, for relatively wide bandgap metal based semiconductors [42,58–61]. Interestingly, despite extensive possibility, this dye-assisted protocol has never been explored for POP-based photochemistry. We postulate that a fraction of MB from the mixed dye solution got adsorbed onto the polymer surface which, itself being photoresponsive, got excited upon visible light illumination. The excited electrons were then injected from the conduction band of MB to that of the photocatalyst. In this way, the adsorbed dye worked as an antenna molecule and the polymer as an electron carrier to open up a unique route for visible light harvesting. The fact that POP-2 can remove MO even in the presence of RhB, further confirms the possibility of this secondary mechanism. Moreover, the photoactivity pattern of POP-1 towards degradation of MB + MO also suggests the presence of a dye-assisted mechanism along with conventional catalyst-sensitized pathway for both materials.

Once the photoexcited electrons are injected into the CB of POPs, they left with essentially two options: i) react with available O_2 to form $O_2^-\cdot$ and/or $^1O_2$ as already been described, or ii) travel back to $dye\cdot^+$. Nonetheless, being energetically unfavourable, the latter pathway proceeds extremely slow [58]. In other words, due to efficient separation of the excitons in the dye sensitized protocol, chances of radiative quenching through electron hole recombination ceases leading to a particularly fast forward-reaction yielding ROS. This theory agrees well with the observed degradation of MO in an exceptionally rapid manner from the MB + MO mixtures. Since the excitons are already separated and chances of recombination are rare, addition of an external hole scavenger was expected to show only a nominal effect on overall reaction rate, if the dye-assisted reaction protocol is to be considered as the only mechanistic way. However, the role of the hole scavengers in the degradation pathway, as mentioned earlier, clearly demonstrated that suppressing photoexcited electron-hole recombination effectively

increases the reaction rate in many folds, inferring an obvious and prudent evidence of direct photocatalysis occurring through the activation of the POP-semiconductors. Increase in the EPR signal intensity of the photocatalysts after exposing to light, and spin-trapping of the generated ROS also supports their direct photoresponsive activity. Based on these two distinct features, it can be concluded that the POP-catalysts are able to manifest both conventional and adsorbed dye-sensitized mechanistic activities simultaneously.

In order to provide a direct proof of this otherwise intuitional dual mechanism theory, we further employed POP-2 for the degradation of a MB + MO mixture under visible light illumination with a 600 nm cut-on filter. As evident from the UV–vis spectra of the dye solutions and the catalyst, using a 600 nm cut-on filter was anticipated to excite only the n–π* band of MB selectively, while the low absorption cross-section of POP-2 in this region was expected to impart only a nominal effect on overall degradation. In other words, only the dye-assisted mechanism should have been perceived under such protocol with a minimum contribution from the direct catalyst sensitization. As expected, switching off the catalyst remained successful and a complete removal of MO was observed within 1 h with a minimal decrease in MB concentration (Fig. S20). This observation clearly confirmed that degradation of MO in the binary mixture was achieved by an adsorbed dye-assisted protocol, while direct catalyst sensitization was responsible for the removal of MB, i.e. the catalysts were manifesting both mechanisms simultaneously in the reaction media.

We designed this study as a proof-of-concept that, engineered synthesis of POP photocatalysts possessing energy gaps in a borderline region between narrow and wide bandgap semiconductors should, in principle, impart both conventional as well as substrate sensitized photoresponsive behaviour into a single semiconductor skeleton (Fig. 12). Gladly, demonstration of two different mechanisms by POPs made us able to provide a supplementary proof for the validation of this theory. It is to be noted that simultaneous presence of both mechanisms under UV-irradiation by TiO_2-based photocatalysts were mentioned before, though no direct experimental proof has been presented yet [86–89]. Reusability of the catalytic systems is another important aspect of heterogeneous catalysts for their economic and sustainable utilization. We iterated degradation of RhB with POP-1 as a test reaction for five consecutive times and observed only a slight overall decrease in degradation efficiency (Fig. S23) indicating a good recyclability of the catalyst. ATR-FTIR and UV–vis absorption spectra of the reused polymers match well with the freshly prepared catalysts confirming the retention of their core structures (Figs. S24–S26).

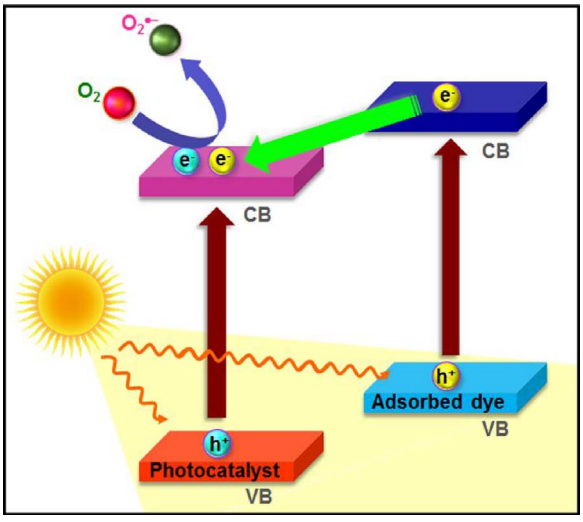

Fig. 12. Schematic representation of the photocatalytic mechanism demonstrated by POPs working under both visible light and natural sunlight.

Table 2
Degradation efficiency and reaction completion time of different dyes catalysed by POP-1 under natural sunlight irradiation.

Dye	Degradation efficiency (%)	Time (min)
RhB	> 99	45
MB	> 99	30
CR	96	45
MO	74	150

4.4. Natural sunlight-induced dye degradation

While the use of an artificial visible light in the laboratory is convenient for the development of any sustainable photocatalytic system, natural solar irradiation conditions are always unique [49]. Therefore retention of the catalytic ability of the material under natural sunlight is considered as the ultimate goal for the real life field applications. It is depicted in the UV–vis absorption spectra of the polymers that both materials retain substantial absorbance to cover a wide portion of natural solar irradiance, with POP-1 featuring relatively higher coverage. This result is indicative of its feasibility to demonstrate natural sunlight promoted photocatalysis. With this idea, we subjected POP-1 for degrading these four dyes in outdoor conditions on a partly sunny day with scattered cloud cover. Initial and final absorption of the dye solutions were measured and shown in Figs. S21 and S22 . We were delighted to observe that our catalyst demonstrated an impressive performance in natural solar irradiation, better than that in artificially simulated visible light induced condition. The specific degradation efficiencies and corresponding reaction times documented in Table 2 can clearly highlight this superior photoactivity.

5. Conclusion

In summary, tailored synthesis of two conjugated hierarchical POP networks employing high dilution technique resulted in low-density solid catalysts possessing impressive surface area, gas adsorption ability and dispersibility. Owing to this synthetic technique, large mesopores were generated in both polymers which make them viable candidates for heterogeneous catalysis by increasing overall mass-transport. Moreover, the materials exhibited wide UV–vis absorption bands covering a significant portion of the natural solar spectrum. The catalysts almost quantitatively degraded cationic and anionic dye-pollutants (RhB, MB, CR and MO) from their aqueous solutions with exceptionally rapid reaction rates in a variable pH range from 2 to 10 under visible light illumination. More importantly, the activity remained unaltered even at outdoor condition with natural sunlight. On top of this excellent photoactivity, the catalytic systems possessing borderline bandgaps demonstrated their unprecedented ability to simultaneously follow two different mechanistic protocols: the conventional catalytic sensitization way, and another substrate-sensitized secondary pathway. A novel time depended selective sequential degradation was also perceived. The study further suggested that utilization of special photoactive units is not always a necessity to impart photocatalytic behaviours in POP skeletons, but strategic synthesis may also play an important role. Retention of excellent photoactivity under natural sunlight illumination, impressive recyclability, and complete depletion of contaminant concentrations even in a multi-component mixed pollutant probe without the use of any additional peroxide reagents inevitably suggest the expedient possibility of the POPs as useful, economic, green and sustainable catalysts for efficient environmental remediation.

Acknowledgement

The authors would like to acknowledge State Key Laboratory of Advanced Technology for Materials Synthesis and Processing, Wuhan

University of Technology and the Chinese Scholarship Council (CSC) for the financial support of J.C. and I.N. for their Ph.D. grants 2014GXZ323 and 2014GXZ328 respectively. The authors also acknowledge Dr. Aiwen Lei and Shengchun Wang, Wuhan University, for EPR analysis; and Dr. Hussein A. Younus, Wuhan University of Technology, for his valuable help with cyclic voltammogram experiment. F.V. acknowledges the support from the Tomsk Polytechnic University Competitiveness Enhancement Program grant.

Appendix A. Supplementary data

Supplementary data associated with this article can be found, in the online version, at https://doi.org/10.1016/j.apcatb.2018.01.032.

References

[1] A. Mills, R.H. Davies, D. Worsley, Chem. Soc. Rev. 22 (1993) 417.
[2] A. Di Paola, E. Garcia-Lopez, G. Marci, L. Palmisano, J. Hazard. Mater. 211–212 (2012) 3.
[3] Y. Qu, X. Duan, Chem. Soc. Rev. 42 (2013) 2568.
[4] H. Tong, S. Ouyang, Y. Bi, N. Umezawa, M. Oshikiri, J. Ye, Adv. Mater. 24 (2012) 229.
[5] J. Luo, X. Zhang, J. Zhang, ACS Catal. 5 (2015) 2250.
[6] Y. Xu, S. Jin, H. Xu, A. Nagai, D. Jiang, Chem. Soc. Rev. 42 (2013) 8012.
[7] J.X. Jiang, F. Su, A. Trewin, C.D. Wood, N.L. Campbell, H. Niu, C. Dickinson, A.Y. Ganin, M.J. Rosseinsky, Y.Z. Khimyak, A.I. Cooper, Angew. Chem. Int. Ed. 46 (2007) 8574.
[8] A. Thomas, Angew. Chem. Int. Ed. 49 (2010) 8328.
[9] P. Kaur, J.T. Hupp, S.T. Nguyen, ACS Catal. 1 (2011) 819.
[10] R. Dawson, A.I. Cooper, D.J. Adams, Prog. Polym. Sci. 37 (2012) 530.
[11] D. Wu, F. Xu, B. Sun, R. Fu, H. He, K. Matyjaszewski, Chem. Rev. 112 (2012) 3959.
[12] F. Vilela, K. Zhang, M. Antonietti, Energy Environ. Sci. 5 (2012) 7819.
[13] X. Zou, H. Ren, G. Zhu, Chem. Commun. 49 (2013) 3925.
[14] M. Rose, ChemCatChem (2014) 1166.
[15] Y. Zhu, H. Yang, Y. Jin, W. Zhang, Chem. Mater. 25 (2013) 3718.
[16] Q. Lin, J. Lu, Z. Yang, X.C. Zeng, J. Zhang, J. Mater. Chem. A 2 (2014) 14876.
[17] J. Lu, J. Zhang, J. Mater. Chem. A 2 (2014) 13831.
[18] Y. Kang, Y. Yang, L.-C. Yin, X. King, G. Liu, H.-M. Cheng, Adv. Mater. 27 (2015) 4572.
[19] Y. Kang, Y. Yang, L.-C. Yin, X. King, L. Wang, G. Liu, H.-M. Cheng, Adv. Mater. 28 (2016) 6471.
[20] J. Weber, A. Thomas, J. Am. Chem. Soc. 130 (2008) 6334.
[21] Y. Xu, L. Chen, Z. Guo, A. Nagai, D. Jiang, J. Am. Chem. Soc. 133 (2011) 17622.
[22] J. Liu, K.K. Yee, K.K. Lo, K.Y. Zhang, W.P. To, C.M. Che, Z. Xu, J. Am. Chem. Soc. 136 (2014) 2818.
[23] L. Chen, Y. Honsho, S. Seki, D. Jiang, J. Am. Chem. Soc. 132 (2010) 6742.
[24] X. Liu, Y. Xu, D. Jiang, J. Am. Chem. Soc. 134 (2012) 8738.
[25] M.G. Schwab, M. Hambergur, X. Feng, J. Shu, H.W. Spiess, X. Wang, M. Antonietti, K. Mullen, Chem. Commun. 46 (2010) 8932.
[26] J.H. Park, K.C. Ko, N. Park, H.-W. Shin, E. Kim, N. Kang, J. Hong Ko, S.M. Lee, H.J. Kim, T.K. Ahn, J.Y. Lee, S.U. Son, J. Mater. Chem. A 2 (2014) 7656.
[27] H. Zolinger, Colour Chemistry-Synthesis, Properties of Organic Dyes and Pigments, VCH publishers, New York, 1987, p. 92.
[28] D. Schowanek, K. Fox, M. Holt, F. Schroeder, Water Sci. Technol. 43 (2001) 179.
[29] C. Novotny, N. Dias, A. Kapanen, K. Malachova, M. Vandrovcova, M. Itavarra, N. Lima, Chemosphere 63 (2006) 1436.
[30] P.Y. Wu, Y.H. Liu, Y. Li, M. Jiang, X.L. Li, Y.H. Shi, J. Wang, J. Mater. Chem. A 4 (2016) 16349.
[31] S. Ameena, M. Akhtarb, Y. Kim, H. Shina, Appl. Catal. B: Environ. 103 (2011) 136.
[32] Y.R. Luo, Comprehensive Handbook of Chemical Bond Energies, CRC Press, China, 2005.
[33] W. Liu, L. Liu, C. Liu, Y. Hao, H. Yang, B. Yuan, J. Jiang, Biochem. Eng. J. 110 (2016) 115.
[34] A.A. Telke, S.-W. Kim, S.P. Govindwar, Folia Microbiol. 57 (2012) 115.
[35] A.A. Ahmad, B.H. Hameed, J. Hazard. Mater. 172 (2009) 1538.
[36] L.L. Xu, X.F. Li, J.Q. Ma, Y.Z. Wen, W.P. Liu, Appl. Catal. A 485 (2014) 91.
[37] J.X. Chen, L.Z. Zhu, Catal. Today 126 (2007) 463.
[38] M.F. Hou, L. Liao, W.D. Zhang, X.Y. Tang, H.F. Wan, G.C. Yin, Chemosphere 83 (2011) 1279.
[39] I.K. Konstantinou, T.A. Albanis, Appl. Catal. B: Environ. 49 (2004) 1.
[40] H.D. Li, Y.H. Sang, S.J. Chang, X. Huang, Y. Zhang, R.S. Yang, H.D. Jiang, H. Liu, Z.L. Wang, Nano Lett. 15 (2015) 2372.
[41] Y. Yang, H.L. Zhang, S.M. Lee, D.S. Kim, W.B. Hwang, Z.L. Wang, Nano Lett. 13 (2013) 803.
[42] C. Chen, W. Ma, J. Zhao, Chem. Soc. Rev. 39 (2010) 4206.
[43] X. Li, J. Wang, Y. Men, Z. Bianc, Appl. Catal. B: Environ. 187 (2016) 115.
[44] X. Hu, C. Hu, R. Wang, Appl. Catal. B: Environ. 176–177 (2015) 637.
[45] G. Ciamician, Science 36 (1912) 385.
[46] D.M. Schultz, T.P. Yoon, Science 343 (2014) 1239176.
[47] L.A. Romero, D.A. Nicewicz, Chem. Rev. 116 (2016) 10075.
[48] C.K. Prier, D.A. Rankic, D.W.C. MacMillan, Chem. Rev. 113 (2013) 5322.
[49] D. Cambie, F. Zhao, V. Hessel, M.G. Debije, T. Noel, Angew. Chem. Int. Ed. 56 (2017) 1050.
[50] X. Liu, J. Iocozzia, Y. Wang, X. Cui, Y. Chen, S. Zhao, Z. Li, Z. Lin, Energy Environ. Sci. 10 (2017) 402.
[51] C.-C. Wang, J.-R. Li, X.-L. Lv, Y.-Q. Zhang, G. Guo, Energy Environ. Sci. 7 (2014) 2831.
[52] R. Rossetti, L.E. Brus, J. Am. Chem. Soc. 106 (1984) 4336.
[53] A. Hagfeldt, M. Graetzel, Chem. Rev. 95 (1995) 49.
[54] Y. Li, M. Liu, L. Chen, J. Mater. Chem. A 5 (2017) 13757.
[55] B.C. Ma, S. Ghasimi, K. Landfester, F. Vilela, K.A.I. Zhang, J. Mater. Chem. A 3 (2015) 16064.
[56] G. Zhan, H.C. Zeng, Chem. Mater. 28 (2016) 4572.
[57] Y. Cui, J. Briscoe, Y. Wang, N.V. Tarakina, S. Dunn, ACS Appl. Mater. Interfaces 9 (2017) 24518.
[58] T. Wu, G. Liu, J. Zhao, H. Hidaka, N. Serpone, J. Phys. Chem. B 102 (1998) 5845.
[59] H. An, Y. Du, T. Wang, C. Wang, W. Hao, J. Zhang, Rare Met. 27 (2008) 243.
[60] L. Ye, Y. Su, X. Jin, H. Xie, C. Zhang, Environ. Sci.: Nano 1 (2014) 90.
[61] J. Schneider, M. Matsuoka, M. Takeuchi, J. Zhang, Y. Horiuchi, M. Anpo, D.W. Bahnemann, Chem. Rev. 114 (2014) 9919.
[62] R. Dhanabal, S. Velmathi, A. Bose, Catal. Sci. Technol. 6 (2016) 8449.
[63] T. Liu, L. Wang, X. Lu, J. Fan, X. Cai, B. Gao, R. Miao, J. Wang, Y. Lv, RSC Adv. 7 (2017) 12292.
[64] R.B. Carlin, W.O. Forshey Jr., J. Am. Chem. Soc. 72 (1950) 793.
[65] Y. Tezuka, Polym. J. 44 (2012) 1159.
[66] D.J. Brunelle, Polym. Chem. 46 (2008) 1151.
[67] K. Zhou, B. Mousavi, Z. Luo, S. Phatanasri, S. Chaemchuen, F. Verpoort, J. Mater. Chem. A 5 (2017) 952.
[68] N. Kang, J.H. Park, K.C. Ko, J. Chun, E. Kim, H.-W. Shin, S.M. Lee, H.J. Kim, T.K. Ahn, J.Y. Lee, S.U. Son, Angew. Chem. Int. Ed. 52 (2013) 6228.
[69] M. Thommes, K. Kaneko, A.V. Neimark, J.P. Olivier, F. Rodriguez-Reinoso, J. Rouquerol, K.S.W. Sing, Pure Appl. Chem. 87 (2015) 1051.
[70] B. Ashourirat, P. Arab, A. Verlander, H.M. El-Kaderi, ACS Appl. Mater. Interfaces 8 (2016) 8491.
[71] G. Chang, Z. Shang, T. Yu, L. Yang, J. Mater. Chem. A 4 (2016) 2517.
[72] B.S. Ghanem, M. Hashem, K.D.M. Harris, K.J. Msayib, M. Xu, P.M. Budd, N. Chaukura, D. Book, S. Tedds, A. Walton, N.B. McKeown, Macromolecules 43 (2010) 5287.
[73] R. Gomes, P. Bhanja, A. Bhaumik, Chem. Commun. 51 (2015) 150.
[74] R. Dawson, A.I. Cooper, D.J. Adams, Polym. Int. 62 (2013) 345.
[75] S. Bandyopadhyay, A.G. Anil, A. James, A. Patra, ACS Appl. Mater. Interfaces 8 (2016) 27669.
[76] J. Sun, J. Zhang, M. Zhang, M. Antonietti, X. Fu, X. Wang, Nat. Commun. (2012) 1139.
[77] S. Chen, G. Yang, S. Luo, S. Yin, J. Jia, Z. Li, S. Gao, Y. Shao, K. Yao, J. Mater. Chem. A 5 (2017) 14230.
[78] J. Shen, R. Steinbach, J.M. Tobin, M.M. Nakata, M. Bower, M.R.S. McCoustra, H. Bridle, V. Arrighi, F. Vilela, Appl. Catal. B: Environ. 193 (2016) 226.
[79] J. Lee, Y. Mackeyev, M. Cho, L.J. Wilson, J.-H. Kim, P.J.J. Alvarez, Environ. Sci. Technol. 44 (2010) 9488.
[80] H. Kim, W. Kim, Y. Mackeyev, G.-S. Lee, H.-J. Kim, T. Tachikawa, S. Hong, S. Lee, J. Kim, L.J. Wilson, T. Majima, P.J.J. Alvarez, W. Choi, J. Lee, Sci. Environ. Technol. 46 (2012) 9606.
[81] S.H. Xie, P. Huang, J.J. Kruzic, X.R. Zeng, H.X. Qian, Sci. Rep. 6 (2016) 21947.
[82] Y. Shen, Z. Zhang, K. Xiao, RSC Adv. 5 (2015) 91846.
[83] H.-P. Jing, C.-C. Wang, Y.-W. Zhang, P. Wang, R. Li, RSC Adv. 4 (2014) 54454.
[84] S.C. Yan, Z.S. Li, Z.G. Zou, Langmuir 26 (2010) 3894.
[85] T. Araya, C.-C. Chen, M.-K. Jia, D. Jhonson, R. Li, Y.-P. Huang, Opt. Mater. 64 (2017) 512.
[86] Y.-C. Hsiao, T.-F. Wu, Y.-S. Wang, C.-C. Hu, C. Huang, Appl. Catal. B: Environ. 148–149 (2014) 250.
[87] W. Tian, J. Yin, L. Wei, Q. Shen, R. Bibi, M. Liu, B. Yang, N. Li, J. Zhou, RSC Adv. 7 (2017) 17020.
[88] X. Ji, X. Yuan, J. Wu, L. Yu, H. Guo, H. Wang, H. Zhang, D. Yu, Y. Zhao, ACS Appl. Mater. Interfaces 9 (2017) 24616.
[89] H.A. Ghaly, A.S. El-Kalliny, T.A. Gad-Allah, N.E.A. Abd El-Sattar, E.R. Souaya, RSC Adv. 7 (2017) 12726.
[90] F.F. Dias, A.A.S. Oliveira, A.P. Arcanjo, F.C.C. Moura, J.G.A. Pacheco, Appl. Catal. B: Environ. 186 (2016) 136.
[91] Y. Zhang, F. Gao, B. Wanjala, Z. Li, G. Cernigliaro, Z. Gu, Appl. Catal. B: Environ. 199 (2016) 504.
[92] T. Kanagaraj, S. Thiripuranthagan, Appl. Catal. B: Environ. 207 (2017) 218.
[93] H. Wang, C. Wang, X. Cui, L. Qin, R. Ding, L. Wang, Z. Liu, Z. Zheng, B. Lv, Appl. Catal. B: Environ. 221 (2018) 169.
[94] A.P. Heitmann, P.S.O. Patrício, I.R. Coura, E.F. Pedroso, P.P. Souza, H.S. Mansur, A. Mansur, L.C.A. Oliveira, Appl. Catal. B: Environ. 189 (2016) 141.